Downloaded from jpet.aspetjournals.org at ASPET Journals on January 9, 2024

Treatment of Sulfur Mustard Corneal Injury by Augmenting the DNA Damage Response

(DDR): A Novel Approach

Robert Shalwitz<sup>1</sup>, Tovah Day<sup>2</sup>, Anna Kotsakis Ruehlmann<sup>1</sup>, Lindsay Julio<sup>2</sup>, Shellaina Gordon<sup>2</sup>,

Adrianna Vandeuren<sup>2</sup>, Marian Nelson<sup>4</sup>, Megan Lyman<sup>4</sup>, Kyle Kelly<sup>4</sup>, Amber Altvater<sup>4</sup>, Celinia

Ondeck<sup>4</sup>, Sean O'Brien<sup>4,5</sup>, Tracey Hamilton<sup>4</sup>, Ryan L. Hanson<sup>3</sup>, Kayla Wayman<sup>3</sup>, Alexandrea

Miller<sup>1</sup>, Isaiah Shalwitz<sup>1</sup>, Eric Batchelor<sup>3</sup>, Patrick McNutt<sup>4, 5</sup>

Running Title: Treatment of (SM) Corneal Injury by Augmenting the DDR

Text Pages: 20

Table: 1

Figures: 7

References: 73

Words in Abstract: 249

Words in Introduction: 812

Words in Discussion: 875

Non-Standard Abbreviations:

ADPR - Adenosine diphosphoribose

DDR – DNA Damage Response

DSB – Double Strand Breaks

1

HCEC - human corneal epithelial cells

HR - Homologous Recombination

ICL - Interstrand crosslinks

OCT - optical coherence tomography

SM – Sulfur Mustard

Corresponding Author:

Robert Shalwitz

1275 Kinnear Rd

Columbus OH, 43212

rshalwitz@invirsa.com

Abstract: Sulfur mustard (SM) is a highly reactive organic chemical has been used as a chemical warfare agent and terrorist threat since WWI. The cornea is highly sensitive to SM toxicity and exposure to low vapor doses can cause incapacitating acute injuries. Exposure to higher doses can elicit persistent secondary keratopathies that cause reduced quality of life and impaired or lost vision. Despite a century of research, there are no specific treatments for acute or persistent ocular SM injuries. SM cytotoxicity emerges, in part, through DNA alkylation and double-strand breaks (DSBs). Because DSBs can naturally be repaired by DNA damage response pathways with low efficiency, we hypothesized that enhancing the HR pathway could pose a novel approach to mitigate SM injury. Here we demonstrate that a dilithium salt of adenosine diphosphoribose (INV-102) increases protein levels of p53 and Sirtuin 6, upregulates transcription of BRCA1/2, enhances yH2AX focus formation and promotes assembly of repair complexes at DSBs. Based on in vitro evidence showing INV-102 enhancement of DDR through both p53-dependent and p53-independent pathways, we next tested INV-102 in a rabbit preclinical model of corneal injury. In vivo studies demonstrate a marked reduction in the incidence and severity of secondary keratopathies in INV-102-treated eyes compared to vehicletreated eyes when treatment was started 24 hours after SM vapor exposure. These results suggest DNA repair mechanisms are a viable therapeutic target for SM injury and suggest topical treatment with INV-102 is a promising approach for SM as well as other conditions associated with DSBs.

**Significance Statement**: Sulfur Mustard Gas corneal injury currently has no therapeutic treatment. This study aims to show the therapeutic potential of activating the body's natural DNA Damage Response to activate tissue repair.

## Introduction

Sulfur mustard (SM) is a highly effective vesicant that was first used as a chemical weapon by German forces in Ypres, Belgium on July 12, 1917. SM is typically deployed as a liquid aerosol that volatilizes to a heavier-than-air vapor in a temperature-dependent manner. Liquid or vapor SM readily penetrates the skin, lungs and eye, where it cyclizes to form two highly reactive episulfonium intermediates that alkylate and crosslink DNA and other biological macromolecules Error! Bookmark not defined. (Tilley 1993). The resulting activation of tissue-specific repair processes and generalized inflammation produces a complex injury that progresses at different time scales in different tissue compartments. The eyes are the most sensitive organ to SM toxicity and, consequently, 90% of SM casualties present with ocular comorbidities ranging in severity from mild conjunctivitis to incapacitating corneal lesions (Sidell, Takafuji and Franz 1997, Balali-Mood and Hefazi 2006). Although corneas will heal within 2-6 weeks after lowdose exposure to SM vapor, corneas exposed to high doses can develop debilitating chronic pathologies, such as recurring corneal epithelial lesions, corneal neovascularization, opacity, and progressive corneal degeneration (Mann and Pullinger 1942, Solberg, Alcalay and Belkin 1997, McNutt, Tuznik et al. 2013). Because there are no specific treatments for SM injury, treatment strategies have focused on mitigating the acute injury and managing MGK symptoms, with little effect. Given the lack of treatments, the risk of permanent visual impairment and the potential for mass casualty exposures, there remains an urgent need for medical countermeasures against ocular SM injury.

The high toxicity of SM derives from its physicochemical properties. SM is lipophilic and readily absorbed into biological tissues, where it rapidly alkylates nucleophilic moieties. Within minutes of exposure to physiological conditions, SM rearranges to form a pair of highly reactive episulfonium ions (Tilley, 1993). Each episulfonium ion then reacts with water and/or cellular nucleophiles within seconds. Although SM has been reported to alkylate RNA, proteins, and phospholipids (Black, 1997; Noor, 1999; Gunhan, 2004; Hess, 2007; Mol, 2008; Batal, 2015; Liling, 2021), DNA alkylation is the primary mechanism of SM toxicity (Kircher, 1983; Ludlum, 1986; Fidder, 1994; Shakarjian, 2010). In particular, DNA interstrand crosslinks (ICLs) are highly cytotoxic, leading to replication stress and double-strand breaks (DSBs) through stalled replication forks, abasic hydrolysis or aberrant repair processes (Andreassen, 2009, Deans and West, 2011, Yue, 2015; Richterova, 2019). Because a small number of ICLs are sufficient to elicit p53- and FAS ligand-dependent apoptosis, ICLs are considered the principle toxic event after SM exposure <sup>0</sup>(Dronkert and Kanaar 2001, Matijasevic, Precopio et al. 2001).

Although it was long thought that ICLs were unrepairable, hypersensitivity to ICLs in patients with Fanconi anaemia revealed a novel process to repair ICLs. Detection of ICL by FANCM and associated proteins recruits several DDR systems to the site of the ICL, including components of homologous recombination (HR) pathway, nucleotide excision repair (NER) pathway and translesion synthesis (TLS) pathway. These pathways converge to recruit BRCA1 and BRCA2 complexes to initiate and regulate ICL repair processes (Deans and West, 2011; McNutt, 2023 McNutt, 2020). Under normal conditions this process is inefficient. However, we hypothesized that exogenously enhancing DDR pathways could increase the efficiency of ICL repair and thus reduce SM-induced genotoxic damage.

Previous work indicates that exogenous adenosine diphosphoribose (ADPR) helps to protect against DNA lesions. In preclinical studies, ADPR treatment reduced injury after UV exposure in the skin and accelerated recovery after X-ray exposure in the oral mucosa (Jowsey, 2010) <sup>0</sup>; injury modalities mechanistically similar to SM genotoxicity. ADPR was recently shown to play a critical role in the HR pathway as a metabolic target of NUDT5 (Das, 2010). Separately, ADPR increases levels of p53 by stimulating phosphorylation of serine-15 and serine-20 by p53-related protein kinase (PRPK) (Halie, 2011). This is potentially useful in treatment of SM genotoxic lesions because p53 is the master regulator of most forms of DDR following DNA damage, including detection of DSBs (Speidel, 2015; Ruff and Dillman, 2010; Miciak and Bunz, 2016). Moreover, p53-deficient epithelial cells are more susceptible to SM injury (Ruff and Dillman, 2010) suggesting that p53 plays an intrinsic protective role after SM exposure. Collectively, these data suggest that exogenous ADPR may enhance DDR pathways and protect against SM injury through multiple mechanisms.

Here we test the hypothesis that exogenous ADPR treatment promotes DDR pathways in vitro and enhances recovery from SM injury in a preclinical model of ocular SM exposure. Through protein expression analysis, fluorescence microscopy, and transcriptional profiling, we demonstrate that a dilithium salt of ADPR activates p53-dependent and p53-independent DDR pathways and elicits functional and molecular changes consistent with enhanced DSB repair. Furthermore, we show topical administration of ADPR significantly improves recovery in a well-described rabbit corneal SM vapor exposure model (McNutt, Hamilton et al., 2012; McNutt, Lyman et al., 2012; McNutt, 2016). Our studies suggest that exogenous treatment with ADPR can promote recovery from SM and potentially other radiomimetic injuries through widespread activation of DDR pathways.

## **Materials and Methods:**

Ethics statement and disclaimers. Animal studies were approved by the Animal Care and Use Committee (USDA certificate number 51-F-0006) at the United States Army Medical Research Institute of Chemical Defense (USAMRICD). All procedures were conducted in accordance with the principles stated in the Guide for the Care and Use of Laboratory Animals and the Animal Welfare Act of 1966 (P.L. 89-544), as amended, and reported consistent with the ARRIVE 2.0 guidelines. USAMRICD has an approved Animal Welfare Assurance Agreement (number A4528-01) on file with the NIH Office of Laboratory Animal Welfare. The views expressed in this manuscript are those of the author(s) and do not reflect the official policy of the Department of Army, Department of Defense, or the U.S. Government.

Animals. Female New Zealand white rabbits (Charles River Laboratories, Germantown, MD) weighing 1.8-2.5 kilograms were housed individually. Rabbits were provided a standard diet with regular enrichment and water *ad libitum* on a 12 h day:night cycle. At described times after SM exposure, rabbits were anesthetized with an intramuscular administration of 15 mg/kg of ketamine and 7 mg/kg of xylazine and euthanized by cardiac injection of sodium pentobarbital. Female rabbits were used in this study because they exhibit a lower incidence of spontaneous epithelial lesions than males (Ruff and Dillman, 2010), reducing the risk of confounding data at later stages of corneal SM injury. The total sample size of 30 rabbits (15 per group) was determined using a two independent sample study design assuming a 33% reduction in corneal thickness during the recurrent edematous lesion, with a maximum corneal thickness of 1500  $\pm$  500  $\mu$ m in the control population ( $\alpha = 0.05$ ,  $\beta = 0.2$ , power = 0.8) (McNutt, Nguyen et al. 2020, McNutt, Kelly et al. 2021). Rabbits were randomly assigned to INV-102 or vehicle treatment groups using the RAND() function in Microsoft Excel and treatments were given concurrently to

avoid sequence bias. Rabbits were exposed in two cohorts, with equal numbers of INV-102 and treated in each cohort. Eyes were clinically scored at 1 d prior to exposure for baseline values and to identify pre-existing corneal lesions, which would have been criteria for exclusion. No rabbits were excluded from the study.

Rabbit ocular vapor exposure procedures. Rabbits were exposed as previously described (McNutt, Lyman et al. 2012). Briefly, sustained-release buprenorphine (0.15 mg/kg, s.c.) was administered 1 d prior to exposure. On the day of exposure, rabbits were anesthetized with an intramuscular administration of 15 mg/kg of ketamine and 7 mg/kg of xylazine. A saturating volume of neat SM (10 μL, 99.95% pure) was applied to Whatman #1 filter paper mounted in the bottom of a 14-mm vapor cap (Caplugs Evergreen #300-1006-020) fit with a rubber O-ring (MSC Industrial Supply Company, Melville, NY) using gel-based glue (Loctite, Düsseldorf, Germany) to prevent mechanical damage to the corneal surface and restrict lateral diffusion of SM. The cap was inverted onto rabbit eyes for 30–150 s. Two minutes after removal of the vapor cap, eyes were flushed with 10 mL of sterile saline to remove residual SM. Rabbits were returned to their cages, observed until sternal, and provided food and water *ad libitum*. Animals were monitored daily for signs of pain and distress and given sustained-release buprenorphine as needed.

Clinical scoring. Corneas were clinically evaluated prior to SM vapor exposure, 1 d after exposure and on a weekly basis thereafter. Clinical evaluations involved topical fluorescein exclusion assays, optical coherence tomography (OCT) and slit lamp evaluations. Corneas were scored for extent of corneal thickness, corneal opacity, neovascularization and epithelial lesions

by at least two blinded observers using a previously described rubric (Holve, 2011) The presence of corneal epithelial lesions was assessed using blue light photography of eyes 1 min after topical administration of 25 μL fluorescein eye drops (Patterson Veterinary, Greeley, CO). Stromal retention of fluorescein indicates disrupted epithelial integrity. For optical coherence tomography (OCT), two-dimensional scans of the cornea were collected from awake rabbits using a Telesto Spectral Domain Imaging System (Thorlabs; Newton, NJ, USA). Horizontal scans (14.5 mm wide x 2.5 mm deep, lateral resolution 20 μm) of the central cornea were collected at 76 kHz. One A-scan by 16 B-scans were averaged to produce a single image with a fixed pixel size of 4.91 μm x 4.91 μm. Images were processed using Image Field Correction to reduce false curvature and an under-sampling filter to reduce background noise. Central corneal thickness was measured using ImageJ and multiplied by a scaling factor of 0.727 to compensate for corneal refraction. No data points were excluded from the study.

Histopathology. Ten weeks after SM vapor exposure, rabbits were euthanized by intramuscular injection of 15 mg/kg ketamine and 7.5 mg/kg xylazine (Patterson Vet Supply, Loveland, CO) followed by intracardiac injection of 100-150 mg/kg pentobarbital (Patterson Vet Supply). Exposed eyes were enucleated and fixed via infusion of 0.01% glutaraldehyde/10% formalin into the anterior chamber followed by immersion fixation in the same fixative for 5 days. The fixed globe was hemisected by cutting through the center of the cornea and optic nerve. The lens was removed from the hemisected eye and the remaining globe was embedded in paraffin. Sections (8 μm) were rehydrated, stained using hematoxylin and eosin (H&E) and corneas were photographed for histological analysis. No data points were excluded from the study.

**INV-102.** INV-102 (dilithium salt of ADPR) was synthesized using an alkaline method to remove nicotinamide from nicotinamide adenine dinucleotide (NAD+). INV-102 was then isolated and purified to 73.4% (w/w). Area percent (a/a) purity by high pressure liquid chromatography was 92%. Principle impurities (in order of amount) were ethanol, water, nicotinamide, NAD+, adenosine monophosphate and ribose phosphate.

Immunoblot. Human corneal epithelial cells (ATCC® PCS-700-010<sup>TM</sup>) were grown to 80-90% confluency in ATCC Corneal Epithelial Cell Basal Medium (ATCC® PCS-700-030TM) at 37°C in 5% CO2, washed twice with sterile phosphate buffered saline (PBS), and cultured for 2 h at 37°C in serum-free medium. The medium was aspirated and cells were treated with 60 µM INV-102 in serum-free media for 15, 30, 60 or 120 minutes. At each time point, the medium was aspirated, cells were washed twice with ice cold PBS, lysed in ice-cold cell lysis buffer and rotated end-over-end at 4°C for 30 min. Lysates were clarified by centrifugation at 14,000g for 30 min at 4°C and the total protein concentration was measured using spectrophotometric methods. Cell lysates were prepared in 2x Laemmli sample buffer and boiled at 95 °C for 5 minutes. Total protein (40 µg) was loaded per well, separated on an 8% tris-glycine gel and transferred to nitrocellulose. After blocking the blot for 1 hour at room temperature in 3% BSA in a standard mixture of tris-buffered saline and Polysorbate 20 (TBST), primary antibody (anti-Pax6 antibody [PAX6496] from Abcam, Inc.; or anti-cytokeratin 12) was added in blocking buffer and incubated overnight at 4°C. The blot was washed 3 times with TBST and HRP-linked secondary antibody added at 1:2000 for 40 minutes at room temperature. The blot was again washed 3 times with TBST and developed with ECL reagents for 1 minute. Images were

obtained with ChemiDocIt Imager (UVP, Upland CA) and analyzed with VisionWorks Software (UVP, Upland CA).

Live cell imaging. hTERT RPE-1 retinal pigmented epithelial cells (ATCC CRL-4000) were maintained at 37°C and 5% CO<sub>2</sub> in RPMI media containing 10% fetal bovine serum (FBS), 1% antibiotic-antimycotic solution (Corning 30-004-CI). hTERT RPE-1 cells expressing p53-Venus and histone H2B-mRuby were maintained under comparable conditions in medium supplemented with 400 μg/mL neomycin (G418), and 10 μg/mL hygromycin. For live-cell imaging, cells were plated into glass-bottom dishes (Mattek) and were imaged 24 h after plating. 2 h prior to imaging, medium was replaced with transparent medium lacking riboflavin and phenol red (Thermo Fisher) and supplemented with 2% fetal bovine serum (FBS), 100 U/mL penicillin G, 100 mg/mL streptomycin sulfate, and 250 ng/mL amphotericin B (Corning). Images were acquired on a Nikon TiE inverted fluorescence microscope equipped with an automatic focus correction system and the iXon Ultra 888 EMCCD Camera (ANDOR Technology Ltd). The Nikon TiE fluorescent microscope was adapted for long-term time-lapse microscopy through the addition of an environmental chamber that maintains a constant environment of 37°C, 5% CO2, and 40% humidity. Images were acquired with a 20x plan apo objective (NA 0.75) every 20 min over a 24-hour period. At the start of the image acquisition, 50 µM INV-102 was added to the cell medium of the active cell dish. After 4 h of imaging, active medium was aspirated and replaced with fresh imaging medium without INV-102. Cell medium was not changed for untreated control cells. The mRuby filter set contained filters of 540-580 nm for the excitation light, 585 nm for the dichroic beam splitter, and 593-668 nm for the emission light (Chroma). The Venus filter set contained filters of 488-512 nm for the excitation light, 520 nm

for the dichroic beam splitter, and 532-554 nm for the emission light (Chroma). Images were analyzed using NIS-Elements software (Nikon) and custom written ImageJ (NIH) and MATLAB software (Mathworks), which is available upon request (E. Batchelor).

qPCR. hTERT RPE-1 cells were seeded on 35-mm dishes and grown to 50% confluence (approximately 24 h) in RPMI media containing 10% fetal bovine serum (FBS), 1% antibioticantimycotic solution (Corning 30-004-CI). Cells were treated with 50 µM INV-102 in growth medium for 4 h, washed with fresh medium, and cultured for up to 24 h. Cells were harvested by scraping at 0, 4, 8 and 24 h after INV-102 addition, pelleted and flash frozen in a dry ice-ethanol bath. mRNA was isolated from cell pellets using the QIAGEN RNeasy plus kit (QIAGEN, 74134) according to manufacture specifications. RNA concentration was determined by Nanodrop (Thermo Fisher) and cDNA was prepared using the High-Capacity cDNA Reverse Transcription kit in 20 µl reactions (Thermo Fisher, 4374966) according to manufacturer specifications. After cDNA generation, the final volume was brought to 100 μl. RT-PCR was performed in 10 µl reactions containing 5 µl Maxima SYBR green master mix (Thermo Fisher, K0222), 2 μL H<sub>2</sub>O, 2 μl cDNA, and 1 μl of 10 μM specific primers (Table 1). For each individual biological replicate, we ran three plates of qRT-PCR reactions for each gene of interest, and we measured on-plate GAPDH levels as a normalization control. Log 2-fold change was quantified by  $\Delta\Delta$ Ct, comparing each time point to the expression at time zero. Data presented as mean log 2-fold change ±SEM. All experiments were performed using three biological replicates.

Quantitation of homologous recombination. U2OS cells containing the DR-GFP assay targeted to the AAVS1 locus (CRL-3455, ATCC) were cultured in DMEM (Gibco) supplemented with 10% FBS and 50 U/mL penicillin and 50 ng/mL streptomycin (Gibco). Cells were treated at the indicated doses of Olaparib (Selleck Chem, S1060) and Bleomycin (Alfa Aesar, AAJ60727MA). Cells were treated with the indicated dose of INV-102 and 16 hours later were infected with Adenovirus (Ad) I-SceI at 2 x 10 9 PFU/mL (generous gift from R. Hromas, University of Florida). At 48 h post-infection, cells were analyzed using an Attune NxT flow cytometer. As a control for adenoviral infection, cells were infected with Ad-β-galactosidase. At the indicated times following bleomycin treatment, cells were pre-extracted with 25 mM HEPES, pH 7.4, 50 mM NaCl, 1 mM EDTA, 3 mM MgCl 2, 300 mM sucrose, and 0.5% Triton X-100 for 5 minutes on ice. Cells were fixed with 4% paraformaldehyde for 12 minutes at room temperature, washed twice with PBS with 1% FBS for blocking and co-stained for 16 hrs at 4C with gamma H2AX S139 (20E3, Cell Signaling) at a dilution of 1:500. Cells were washed with PBS containing 1% FBS and stained for 2 hrs in the dark at room temperature with Alexa Fluor 488 goat anti-mouse (eBioscience) at a dilution of 1:1000. Slides were prepared with mounting media with DAPI (Vectashield). Images were acquired using a Zeiss AxioObserver microscope with a 40X objective. Acquisition software and image processing used the Zeiss AxioVision software package (Zeiss Imaging). Images were analyzed with the US National Institutes of Health Image J FIJI program. All images were acquired in Northeastern University's Institute for Chemical Imaging of Living Systems.

**Statistical analyses**. Prism version 9 (GraphPad Software) was used for statistical analyses. Details of statistical tests and sample sizes are described within the text or figure legend. Unless otherwise stated, data are presented as mean  $\pm$  standard error. Markers of statistical significance are described in corresponding legends.

### **Results**

INV-102 treatment increases p53 protein levels

To assess the potential for INV-102 to treat SM-induced genotoxicity, we first sought to evaluate the effects of INV-102 on p53 levels in human corneal epithelial cells (HCEC). P53 levels were measured via immunoblot following treatment of HCEC with INV-102 for 15, 30, 60 or 120 min. INV-102 treatment increased normalized p53 levels to 313% of no treatment controls within 15 min and 510% by 120 min (Figure 1A), confirming the effects of INV-102 on p53 expression. We also measured the effects of INV-102 on the DSB sensor sirtuin 6 (Sirt6), which recruits ataxia-telangiectasia mutated protein to phosphorylate H2AX at DSBs, thus activating HR and non-homologous end joining repair pathways (Li, 2008; Hu, 2018; Korotkov, 2021). INV-102 increased Sirt6 levels by 155% at 30 minutes before declining to baseline at 120 min (Figure 1B). Finally, we evaluated the transcriptional regulator Pax6, which plays a critical role in maintaining corneal epithelial cells in a properly differentiated state (Hongyun, 2022). INV-102 increased Pax6 levels by 584% (isoform 5A) and 302% (isoform 6) by 60 min after treatment (Figure 1C). Since Pax6 is known to increase cytokeratin 12 expression in corneal epithelial cells, cytokeratin 12 was also evaluated (Batchelor, 2011). Both the monomer and dimer forms of cytokeratin 12 were significantly increased by INV-102 treatment (Figure 1C). Collectively, these data confirmed that INV-102 treatment increased the levels of master regulators of DDR and corneal epithelial cell differentiation in HCEC.

INV-102 treatment leads to stabilization of p53 in individual cells

Immunoblot data confirmed that INV-102 treatment transiently increased p53 levels. Because p53 expression is known to be both highly dynamic and heterogenous (Batchelor 2011; Geva-Zatorsky, 2006), we took advantage of a recombinant RPE-1 epithelial cell line expressing p53-mVenus and histone H2B-mRuby to evaluate the effects of INV-102 treatment on nuclear p53 levels in single cells over 24 h. Cells were treated with INV-102 or vehicle and imaged at 20 min intervals for 24 hours. INV-102 was washed out after 4 h to avoid induction of p53-mediated apoptosis and to evaluate the longitudinal effects of short-term treatment with INV-102 on p53 levels. Addition of INV-102 led to an immediate increase in nuclear p53 levels that remained stable through the 4 h treatment period (Figure 2). p53 levels then increased an additional 200% from 4-12 h before stabilizing and declining. The acute increase in p53 levels within 20 min after INV-102 treatment is consistent with Figure 1A. These data suggest 4 h treatment with INV-102 increases p53 levels for approximately 12 h, similar to other p53 stimuli (Batchelor, 2011; Lahay, 2004).

INV-102 leads to the upregulation of several p53 target genes

To confirm that INV-102 functionally activates the full range of DNA damage responses, we investigated p53-dependent transcriptional programs in response to INV-102 treatment in p53-mVenus-expresing RPE-1 cells. Cells were treated with INV-102 for 4 h, washed with fresh medium and incubated for up to an additional 20 h. RNA was isolated at 0, 4, 8 and 24 h after INV-102 treatment and well-characterized targets of p53 activation were analyzed by qPCR (Figure 2A). Several different patterns were apparent: for example, CDKN1A (p21), PPM1D (WIP1), and BAX showed initial peaks after INV-102 treatment that subsequently declined after INV-102 removal (Figure 3). Others, such as MDM2, BBC3, RRM2B, FANCC, PCNA, MLH1

and MSH2, showed little change at 4 h, but significant declined at later time points. BAX, DD82, RPA and RAD51 were not affected by INV-102 treatment. GADD45A was significantly depressed at 4 and 8 h after treatment. Collectively, these patterns were consistent with p53 induced transcriptional responses that were induced by short term (pulsatile) activation of p53 by ADPR, as shown in Figure 2. While previous studies have shown an inverse relationship between p53 expression and the levels of the DNA DSB repair-associated proteins BRCA1 and BRCA2 (Arizti, 2000), we found INV-102 treatment led to sustained upregulation of both. While the mechanism of BRCA up-regulation requires further investigation, these results suggest INV-102 treatment activates both p53-dependent and p53-independent mechanisms of DNA repair.

INV-102 leads to elevated rates of homologous recombination

The observation that INV-102 treatment increases BRCA1 expression prompted us to test whether INV-102 also enhanced BRCA1 recruitment to sites of DNA DSBs. We examined recruitment of BRCA1 to a CRISPR/Cas9-targeted DSB in the CD4 locus by chromatin immunoprecipitation (ChIP). We selected the *CD4* locus because we previously characterized recruitment of DNA repair factors to this locus (Day, 2017). INV-102 significantly increased BRCA1 recruitment to a site 11 bp from the DSB at the *CD4* locus (Figure 4A). INV-102 also increased recruitment of BRCA1 at sites more distant from the lesion (197 and 2000 bp). These data suggest that INV-102 enhances recruitment of BRCA1 in the vicinity of DNA DSBs.

We next measured homologous recombination (HR) pathway activity using a chromosomally integrated HR reporter (DR-GFP; Figure 4B) (Pierce, 1999) to test whether the increases in BRCA1 recruitment by INV-102 functionally enhances repair efficiency. INV-102 treatment increased the frequency of HR repair of DSBs caused by the I-SceI endonuclease (Figure 4C). Importantly, INV-102 did not alter cleavage levels of the intact locus by I-SceI as detected by

qPCR (Figure 4D), indicating that HR changes did not result from increased cutting by I-SceI in the reporter cassette. Interestingly, inhibition of PARP1 and PARP2 by Olaparib blocked the INV-102-dependent increase in HR, suggesting poly(ADP)ribosylation mediates this effect.

We examined kinetics of γH2AX focus formation as an orthogonal assay for HR activity. Bleomycin induces significantly higher focus formation at 2 h and significantly less at 4 h in INV-102 treated cells vs control (Figure 5A). This suggests INV-102 accelerates repair of DNA DSBs. Because the relative contributions of DSB repair pathways are governed by the cell cycle, we evaluated INV-102 influences on cell cycle dynamics. We observed that cell cycle profiles of vehicle-treated and INV-102-treated cells are indistinguishable (Figure 5B). Taken together, the results suggest that INV-102 promotes HR-mediated repair of DSBs in a manner that is independent of the cell cycle.

# INV-102 mitigates Sulfur Mustard Gas Injury

In light of in vitro data showing INV-102 transiently augments p53 expression and activates both p53-dependent and p53-independent elements of the DSB repair pathway, we tested INV-102 in a preclinical model of ocular SM vapor exposure (McNutt, 2023). Female rabbits were exposed to SM for 90 s using a vapor cap placed directly on the cornea of one eye, producing an estimated vapor dose of 900 mg•min/m³. This vapor dose results in a severe acute lesion within 24 h, involving epithelial sloughing, extensive keratocytosis and partial loss of the corneal endothelial cells under the exposed area. Although the acute lesion appears to heal from 1-2 wk after exposure, over 95% of rabbits subsequently undergo a recurrent edematous lesion characterized by a transient but profound increase in corneal thickness that triggers the emergence of irreversible secondary keratopathies such as fibrosis, neovascularization and opacity (McNutt, Kelly et al., 2021).

To replicate a post-symptomatic treatment model, vehicle or 1% INV-102 was administered topically twice daily for 2 wk, starting 24 h after exposure (total n=15 rabbits per treatment group). Exposed eyes uniformly developed acute corneal lesions within the exposed area by 1 d, as illustrated by fluorescein uptake assays (Figure 6A) and increased corneal thicknesses (Figure 6B). All vehicle-treated animals subsequently developed recurrent corneal lesions after 21 d (defined as an increase in thickness (edema) to ≥ 200% of baseline thickness). Recurrent edematous lesions developed in all vehicle between 21 d and 42 d, leading to increased mean corneal thickness, corneal opacity and corneal fluorescein staining. Although INV-102 treatment had no apparent effect on corneal appearance or clinical metrics during the treatment period, INV-102 treatment significantly reduced mean cornea thickness (Figure 6B) and clinical severity scores starting at 28 d (Figure 6C). In comparison to vehicle rabbits, only 47% (7/15; p=0.002 vs vehicle) of rabbits developed a recurrent edematous lesion through 10 wk. The corresponding improvements in clinical severity scores in INV-102-treated eyes were driven primarily by reduced corneal opacity (Figure 6D) and recurrent epithelial lesions (Figure 6E) in the absence of the recurrent edematous lesion.

The longitudinal effect of INV-102 on corneal thickness and morphology is further illustrated via optical coherence tomography (OCT) imaging in representative eyes (Figure 7A). The emergence of the recurrent edematous lesion involves a frank increase in corneal thickness and the transient development of stromal voids. Although INV-102 eyes show cartographic differences at 42 d and beyond that are indicative of neovascularization and a small degree of fibrosis, the lack of a recurrent edematous lesion through 10 wk is quite stark in comparison to vehicle-treated eyes. Accordingly, although INV-102 eyes exhibit modest morphological abnormalities in optical coherence tomography (OCT) images, their structure is qualitatively

improved compared to vehicle-treated eyes. Post-mortem histological analysis at 10 wk revealed significant improvements in overall corneal structure (Figure 7B) with marked reduction of inflammation, fibrosis and red blood cells in the stroma of INV-102-treated corneas compared to vehicle-treated corneas (Figure 7C). Consistent with reduced neovascularization scores, vessels in INV-102 eyes were diminished in size, length and prevalence than vehicle-treated corneas. Reduced hypercellularization and fibrosis in INV-102-treated corneas is the basis for improved opacity scores compared to vehicle-treated corneas at 10 wk.

### **Discussion**

We evaluated the mechanistic and therapeutic effects of a clinically formulated dilithium salt of adenosine diphosphoribose (INV-102) on DDR pathways in an effort to augment the intrinsic ability of cells to repair ICLs. In mechanistic studies, INV-102 enhanced multiple components of diverse cellular repair and stabilization pathways, including: a) increasing protein levels of p53, Sirtuin 6 and Pax6; b) upregulating transcription of BRCA1 and BRCA2; and c) enhancing γH2AX focus formation and promoting assembly of repair complexes at DSBs. In a preclinical model of ocular SM exposure, INV-102 treatment markedly reduced the incidence and severity of secondary keratopathies compared to vehicle-treated eyes. These results suggest DNA repair mechanisms are a viable therapeutic target for SM injury and suggest topical treatment with INV-102 is a promising approach for SM as well as other conditions associated with DSBs.

One potential method to enhance the DDR system is by modulating p53 activity. However, activation of p53 to achieve a therapeutic effect is challenging. P53 levels accumulate in a series of oscillatory pulses in response to DNA damage (Lahav, 2004; Batchelor, 2008). These pulses are important for p53 regulation of downstream genes (Harton, 2019; Porter, 2016) and

ultimately affect cell fate (Gupta, 2019; Kim, 1993). Excessive or sustained p53 activation leads to cellular senescence and/or apoptosis (Gupta, 2019; Purvis, 2012). Thus, the challenge was to find a short-acting compound that increases p53 activation without inducing cell cycle or apoptotic effects. While ADPR as a component of poly-ADP-ribose chains built by PARP enzymes has been studied extensively, the free monomer ADPR has not been well examined. Two studies demonstrated the mechanisms for ADPR's rapid metabolism to adenosine monophosphate (AMP) after transport into the cell (Gupta, 2019; Kim, 1993). Multiple PARP inhibitors are now FDA-approved in the oncology clinic and others are in development for a variety of diseases, yet almost none of the PARP literature considers the production or function of ADPR monomers. Our study indicates that monomers of ADPR can be actively transported into cells and have a powerful physiological function in regulating the DDR. Not only does ADPR, in the form of INV-102 activate p53, but our data highlights unique aspects of ADPR's response not described for other p53 activators. Aziri et al reports P53 downregulates BRCA1/2 (Arizti, 2000), yet we have shown that ADPR both activates p53 and concurrently upregulates BRCA1 and BRCA2. BRCA1 and BRCA2 are critical regulators of the DSB response and homologous recombination, and we show that ADPR increases homologous recombination and the overall efficiency of DSB repair.

Our observation that ADPR upregulates BRCA1/2 suggests existence of an additional p53-independent and ADPR-responsive HR mechanism. Previous studies suggest that ATP and ADP inhibit MDM2 by allosteric hinderance to the zinc (ring) finger domain of the protein (Poyurovsky, 2003; Priest, 2010). It is likely that ADPR binds in a similar manner to MDM2 and to additional zinc finger proteins (ZNF) involved in DSB repair and ADP-ribosylation. Two such proteins are BARD1 and CTCF. BRCA1 and BARD1 have zinc-chelating RING domains, and

the two proteins assemble into a stable heterodimer through the association of their RING domains. Recruitment of BRCA1/BARD1 to stalled replication forks is known to be dependent on poly-ADPR binding to this heterodimer (Billing, 2018). It is possible that monomers of ADPR are sufficient to stimulate the recruitment of the heterodimer. In addition, the BRCA1/BARD1 heterodimer has been shown to decrease BRCA1 related transactivation of GADD45a which may account for the downregulation of GADD45a seen in this study (Fabbro, 2008). An additional approach may be the binding of ADPR to CTCF zinc fingers which inhibits BRCA1/2 and links to BRCA1/2 inactivation in human breast tumors (Butcher, 2006). Further experiments are required to determine whether these effects might facilitate induction of BRCA1/2 by INV-102.

Although our findings are consistent with the interpretation that INV-102 mitigates SM tissue injury by enhancing multiple DDR pathways, it remains possible that INV-102 improves recovery from SM injury via other means, such as enhancing corneal regeneration during the acute and subacute injury phase. Elucidation of the cellular mechanisms involved in INV-102 activation of DDR pathways will require additional investigation. For example, characterization of the INV-102 interactome may identify a network of cellular factors involved in its unique proregenerative effects. A more complete understanding of the transport of INV-102 into cells and between cells is also important for development of this small molecule as a therapeutic strategy. Finally, detailed assessment of INV-102 effects on DDR activity in corneas following genotoxic injury would significantly improve understanding of the therapeutic benefits observed in our in vivo studies.

In conclusion, our data suggests a model whereby activation of p53 and other DNA response pathways by ADPR significantly enhances cellular and tissue repair of damage by SM. We

suggest that ADPR acts in part by enhancing the DNA damage response to DSBs. Furthermore, ADPR's short half-life may be important to avoid cell cycle and apoptotic effects associated with prolonged p53 activation. Modulation of DNA repair pathways is an area of intense interest for experimental and therapeutic development of genome editing (Yeh, 2019). Our data suggest that INV-102 may be useful in genome editing applications where homology-directed repair is the desired outcome. Collectively, these data establish the therapeutic potential for ADPR for conditions associated with DNA damage.

The authors declare that all the data supporting the findings of this study are contained within the paper.

## **Authorship Contributions:**

Participated in Research design: R. Shalwitz, Day, Kotsakis Ruehlmann, Batchelor, McNutt

Conducted Experiments: Day, Julio, Gordon, Vandeuren, Nelson, Lyman, Kelly, Altvater,
Ondeck, O'Brien, Hamilton, Hanson, Wayman, Kotsakis Ruehlmann, Batchelor, McNutt

Performed Data Analysis: R. Shalwitz, Day, Julio, Gordon, Vandeuren, Nelson, Lyman, Kelly,
Altvater, Ondeck, O'Brien, Hamilton, Hanson, Wayman, Kotsakis Ruehlmann, I. Shalwitz
Batchelor, McNutt

Wrote or contributed to the writing of the manuscript: R. Shalwitz, Day, Kotsakis Ruehlmann, Miller, I. Shalwitz, Batchelor, McNutt

- Andreassen, P. R. and K. Ren (2009). "Fanconi anemia proteins, DNA interstrand crosslink repair pathways, and cancer therapy." <u>Curr Cancer Drug Targets</u> **9**(1): 101-117.
- Arizti, P., Fang, L., Park, I., Yin, Y., Solomon, E., Ouchi, T., Aaronson, S. A., & Lee, S. W. (2000). Tumor suppressor p53 is required to modulate BRCA1 expression. Molecular and cellular biology, 20(20), 7450–7459. https://doi.org/10.1128/MCB.20.20.7450-7459.2000
- Balali-Mood, M. and M. Hefazi (2006). "Comparison of early and late toxic effects of sulfur mustard in Iranian veterans." Basic Clin Pharmacol Toxicol **99**(4): 273-282.
- Baradaran-Rafii, A., M. A. Javadi, F. Karimian and S. Feizi (2013). "Mustard gas induced ocular surface disorders." J Ophthalmic Vis Res **8**(4): 383-390.
- Batal, M., S. Rebelo-Moreira, N. Hamon, P. A. Bayle, S. Mouret, C. Clery-Barraud, I. Boudry and T. Douki (2015). "A guanine-ethylthioethyl-glutathione adduct as a major DNA lesion in the skin and in organs of mice exposed to sulfur mustard." <u>Toxicol Lett</u> **233**(1): 1-7.
- Batchelor E, Loewer A, Mock C, Lahav G. Stimulus-dependent dynamics of p53 in single cells.

  Mol Syst Biol. 2011 May 10;7:488. Doi: 10.1038/msb.2011.20.
- Batchelor E, Mock CS, Bhan I, Loewer A, Lahav G. Recurrent initiation: a mechanism for triggering p53 pulses in response to DNA damage. Mol Cell. 2008 May 9;30(3):277-89. Doi: 10.1016/j.molcel.2008.03.016.
- Billing, D., Horiguchi, M., Wu-Baer, F., Taglialatela, A., Leuzzi, G., Nanez, S. A., Jiang, W., Zha, S., Szabolcs, M., Lin, C.-S., Ciccia, A., & Baer, R. (2018). The BRCT Domains of the BRCA1 and BARD1 Tumor Suppressors Differentially Regulate Homology-Directed Repair and Stalled Fork Protection. Molecular Cell, 72(1), 127-139.e8. https://doi.org/10.1016/j.molcel.2018.08.016

- Black, R. M., R. J. Clarke, J. M. Harrison and R. W. Read (1997). "Biological fate of sulphur mustard: identification of valine and histidine adducts in haemoglobin from casualties of sulphur mustard poisoning." <u>Xenobiotica</u> **27**(5): 499-512.
- Butcher DT, Rodenhiser DI. Epigenetic inactivation of BRCA1 is associated with aberrant expression of CTCF and DNA methyltransferase (DNMT3B) in some sporadic breast tumours. Eur J Cancer. 2007 Jan;43(1):210-9. Doi: 10.1016/j.ejca.2006.09.002. Epub 2006 Oct 27.
- Charni M, Alone-Grinstein R, Molcahdsky A, Rotter V. p53 on the Crossroad Between Regeneration and Cancer. Cell Death and Differentiation. 2017 Jan;24(1):8-14.
- Das T, Mitchell DL, Johns PW, Jorgensen EB, Roy-Alexander D, Shalwitz RA. Protective role of ADP-ribose against ionizing radiation induced oral mucositis and UV-mediated skin damage. Proc Amer Assoc Cancer Res. 2005 May;65(9): 342.
- Day TA, Layer JV, Cleary JP, Guha S, Stevenson KE, Tivey T, S, Schinzel AC, Izzo F, Doench J, Root DE, Hahn WC, Price BD, Weinstock DM. PARP3 is a promoter of chromosomal rearrangements and limits G4 DNA. Nat Commun. 2017 Apr 27;8:15110. Doi: 10.1038/ncomms15110. Erratum in: Nat Commun. 2017 Jun 13;8:15918.
- Deans, A. J., & West, S. C. (2011). DNA interstrand crosslink repair and cancer. Nature Reviews. Cancer, 11(7), 467–480. <a href="https://doi.org/10.1038/nrc3088">https://doi.org/10.1038/nrc3088</a>
- Dronkert, M. L. and R. Kanaar (2001). "Repair of DNA interstrand cross-links." Mutat Res 486(4): 217-247.
- Fabbro M, Henderson BR. BARD1 regulates BRCA1-mediated transactivation of the p21WAF1/CIP1 and Gadd45 promoters. Cancer Lett. 2008 May 18;263(2):189-96. doi: 10.1016/j.canlet.2008.01.001. Epub 2008 Feb 20. PMID: 18243530.

- Fidder, A., G. W. Moes, A. G. Scheffer, G. P. van der Schans, R. A. Baan, L. P. de Jong and H. P. Benschop (1994). "Synthesis, characterization, and quantitation of the major adducts formed between sulfur mustard and DNA of calf thymus and human blood." <a href="#">Chem Res</a>
  <a href="#">Toxicol 7(2): 199-204.</a>
- Geva-Zatorsky N, Rosenfeld N, Itzkovitz S, Milo R, Sigal A, Dekel E, Yarnitzky T, Liron Y, Polak P, Lahav G, Alon U. Oscillations and variability in the p53 system. Mol Syst Biol. 2006;2:2006.0033. doi: 10.1038/msb4100068. Epub 2006 Jun 13.
- Gomez-Lazaro M, Fernandez-Gomez FJ, Jordán J. p53: twenty five years understanding the mechanism of genome protection. J Physiol Biochem. 2004 Dec;60(4):287-307. Doi: 10.1007/BF03167075.
- Gunhan, O., B. Kurt, T. Karayilanoglu, L. Kenar and B. Celasun (2004). "Morphological and immunohistochemical changes on rat skin exposed to nitrogen mustard." Mil Med

  169(1): 7-
- Gupta, A., Shah, K., Oza, M. J., & Behl, T. (2019). Reactivation of p53 gene by MDM2 inhibitors: A novel therapy for cancer treatment. Biomedicine & Pharmacotherapy, 109, 484–492. https://doi.org/10.1016/j.biopha.2018.10.155
- Hagemann, J. H., Thomasova, D., Mulay, S. R., & Anders, H.-J. (2013). Nrf2 signalling promotes ex vivo tubular epithelial cell survival and regeneration via murine double minute (MDM)-2. Nephrology Dialysis Transplantation, 28(8), 2028–2037. <a href="https://doi.org/10.1093/ndt/gft037">https://doi.org/10.1093/ndt/gft037</a>
- Haile JD, Kennelly PJ. The activity of an ancient atypical protein kinase is stimulated by ADP-ribose in vitro. Arch Biochem Biophys. 2011 Jul;511(1-2):56-63. Doi: 10.1016/j.abb.2011.04.006. Epub 2011 Apr 19.

- Harton, M. D., Koh, W. S., Bunker, A. D., Singh, A., & Batchelor, E. (2019). P53 pulse modulation differentially regulates target gene promoters to regulate cell fate decisions. *Molecular Systems Biology*, 15(9). https://doi.org/10.15252/msb.20188685
- Hess, J. F. and P. G. FitzGerald (2007). "Treatment of keratin intermediate filaments with sulfur mustard analogs." <u>Biochem Biophys Res Commun</u> **359**(3): 616-621.
- Holve DL, Mundwiler KE, Pritt SL (2011) Incidence of spontaneous ocular lesions in laboratory rabbits. Comp Med 61(5):436-40
- Hu, X., Zhu, S., Liu, R., Miller, J. D., Merkley, K., Tilton, R. G., & Liu, H. (2018). Sirt6 deficiency impairs corneal epithelial wound healing. Aging, 10(8), 1932–1946. <a href="https://doi.org/10.18632/aging.101513">https://doi.org/10.18632/aging.101513</a>
- Javadi, M. A., S. Yazdani, M. R. Kanavi, M. Mohammadpour, A. Baradaran-Rafiee, M. R.
  Jafarinasab, B. Einollahi, F. Karimian, M. Zare, M. Naderi and H. M. Rabei (2007).
  "Long-term outcomes of penetrating keratoplasty in chronic and delayed mustard gas keratitis." <a href="Cornea">Cornea</a> 26(9): 1074-1078
- Javadi, M. A., S. Yazdani, M. R. Kanavi, M. Mohammadpour, A. Baradaran-Rafiee, M. R.
  Jafarinasab, B. Einollahi, F. Karimian, M. Zare, M. Naderi and H. M. Rabei (2007).
  "Long-term outcomes of penetrating keratoplasty in chronic and delayed mustard gas keratitis." <a href="Cornea">Cornea</a> 26(9): 1074-1078.
- Johns, P., Pereira, S. L., Leonard, A. E., Mukerji, P., Shalwitz, R. A., Dowlati, L., Phillips, R. R., Bergana, M. S., Holton, J. D., & Das, T. (2007). Cytoprotective Agent in Lactobacillus bulgaricus Extracts. *Current Microbiology*, *54*(2), 131–135. https://doi.org/10.1007/s00284-006-0256-6

- Jowsey PA, Williams FM, Blain PG. DNA damage responses in cells exposed to sulphur mustard. Toxicol Lett. 2012 Feb 25;209(1):1-10. Doi: 10.1016/j.toxlet.2011.11.009. Epub 2011 Nov 18.
- Jowsey, P. A., Williams, F. M., & Blain, P. G. (2010). The role of homologous recombination in the cellular response to sulphur mustard. Toxicology Letters, 197(1), 12–18. https://doi.org/10.1016/j.toxlet.2010.04.020
- Kim, U. H., Han, M. K., Park, B. H., Kim, H. R., & An, N. H. (1993). Function of NAD glycohydrolase in ADP-ribose uptake from NAD by human erythrocytes. Biochimica et Biophysica Acta, 1178(2), 121–126.
- Kircher, M. and M. Brendel (1983). "DNA alkylation by mustard gas in yeast strains of different repair capacity." Chem Biol Interact 44(1-2): 27-39.
- Kitazawa, K., Hikichi, T., Nakamura, T., Sotozono, C., Kinoshita, S., & Masui, S. (2017). PAX6 regulates human corneal epithelium cell identity. Experimental Eye Research, 154, 30–38. <a href="https://doi.org/10.1016/j.exer.2016.11.005">https://doi.org/10.1016/j.exer.2016.11.005</a>
- Korotkov, A., Seluanov, A., & Gorbunova, V. (2021). Sirtuin 6: Linking longevity with genome and epigenome stability. Trends in Cell Biology, 31(12), 994–1006. <a href="https://doi.org/10.1016/j.tcb.2021.06.009">https://doi.org/10.1016/j.tcb.2021.06.009</a>
- Lahav G. The strength of indecisiveness: oscillatory behavior for better cell fate determination. Sci STKE. 2004 Dec 21;2004(264):pe55. Doi: 10.1126/stke.2642004pe55.
- Li, W., Chen, Y.-T., Hayashida, Y., Blanco, G., Kheirkah, A., He, H., Chen, S.-Y., Liu, C.-Y., & Tseng, S. (2008). Down-regulation of Pax6 is associated with abnormal differentiation of corneal epithelial cells in severe ocular surface diseases. The Journal of Pathology, 214(1), 114–122. https://doi.org/10.1002/path.2256

- Ludlum, D. B., S. Kent and J. R. Mehta (1986). "Formation of O6-ethylthioethylguanine in DNA by reaction with the sulfur mustard, chloroethyl sulfide, and its apparent lack of repair by O6-alkylguanine-DNA alkyltransferase." <u>Carcinogenesis</u> 7(7): 1203-1206.
- Luling, R., W. Schmeisser, M. Siegert, H. Muckter, A. Dietrich, H. Thiermann, T. Gudermann, H. John and D. Steinritz (2021). "Identification of creatine kinase and alpha-1 antitrypsin as protein targets of alkylation by sulfur mustard." Drug Test Anal **13**(2): 268-282.
- Luo, Q., Beaver, J., Liu, Y., & Zhang, Z. (2017). Dynamics of p53: A Master Decider of Cell Fate. Genes, 8(2), 66–66. https://doi.org/10.3390/genes8020066
- Mann, I. and B. D. Pullinger (1942). "A study of mustard gas lesions of the eyes of rabbits and men (Section of Ophthalmology)." Proc R Soc Med 35(3): 229-244.
- Matijasevic, Z., M. L. Precopio, J. E. Snyder and D. B. Ludlum (2001). "Repair of sulfur mustard-induced DNA damage in mammalian cells measured by a host cell reactivation assay." <u>Carcinogenesis</u> **22**(4): 661-664.
- McNutt PM, Kelly KEM, Altvater AC, et al. (2021) Dose-dependent emergence of acute and recurrent corneal lesions in sulfur mustard-exposed rabbit eyes. Toxicol Lett 341:33-42 doi:10.1016/j.toxlet.2021.01.016
- McNutt, P. (2023). "Progress towards a standardized model of ocular sulfur mustard injury for therapeutic testing." Exp Eye Res 228: 109395.
- McNutt, P. M., D. L. Nguyen, M. R. Nelson, M. E. Lyman, M. M. Eisen, C. A. Ondeck, S. E. Wolfe, K. T. Pagarigan, M. C. Mangkhalakhili, D. M. Kniffin and T. A. Hamilton (2020). "Corneal Endothelial Cell Toxicity Determines Long-Term Outcome After Ocular Exposure to Sulfur Mustard Vapor." <a href="#">Cornea</a> 39(5): 640-648.

- McNutt, P. M., K. M. Tuznik, E. J. Glotfelty, M. R. Nelson, M. E. Lyman and T. A. Hamilton (2016). "Contributions of tissue-specific pathologies to corneal injuries following exposure to SM vapor." <u>Ann N Y Acad Sci</u> **1374**(1): 132-143.
- McNutt, P. M., K. M. Tuznik, E. J. Glotfelty, M. R. Nelson, M. E. Lyman and T. A. Hamilton (2016). "Contributions of tissue-specific pathologies to corneal injuries following exposure to SM vapor." <u>Ann N Y Acad Sci</u> **1374**(1): 132-143.
- McNutt, P., Hamilton, T., Nelson, M., Adkins, A., Swartz, A., Lawrence, R., & Milhorn, D. (2012). Pathogenesis of acute and delayed corneal lesions after ocular exposure to sulfur mustard vapor. Cornea, 31(3), 280–290. https://doi.org/10.1097/ICO.0B013E31823D02CD
- McNutt, P., K. Tuznik, M. Nelson, A. Adkins, M. Lyman, E. Glotfelty, J. Hughes and T. Hamilton (2013). "Structural, morphological, and functional correlates of corneal endothelial toxicity following corneal exposure to sulfur mustard vapor." <a href="Invest Ophthalmol Vis Sci 54(10)">Invest Ophthalmol Vis Sci 54(10)</a>: 6735-6744.
- McNutt, P., M. Lyman, A. Swartz, K. Tuznik, D. Kniffin, K. Whitten, D. Milhorn and T. Hamilton (2012). "Architectural and biochemical expressions of mustard gas keratopathy: preclinical indicators and pathogenic mechanisms." <u>PLoS One</u> 7(8): e42837.
- Miciak, J, Bunz, F. Long story short: p53 mediates innate immunity. Biochim Biophys Acta. 2016 Apr;1865(2): 220-227
- Mol, M. A., R. M. van den Berg and H. P. Benschop (2008). "Proteomic assessment of sulfur mustard-induced protein adducts and other protein modifications in human epidermal keratinocytes." Toxicol Appl Pharmacol **230**(1): 97-108.

- Noort, D., A. G. Hulst, L. P. de Jong and H. P. Benschop (1999). "Alkylation of human serum albumin by sulfur mustard in vitro and in vivo: mass spectrometric analysis of a cysteine adduct as a sensitive biomarker of exposure." Chem Res Toxicol 12(8): 715-721.
- Pierce AJ, Johnson RD, Thompson LH, Jasin M. XRCC3 promotes homology-directed repair of DNA damage in mammalian cells. Genes Dev. 1999 Oct 15;13(20):2633-8. doi: 10.1101/gad.13.20.2633.
- Porter JR, Fisher BE, Batchelor E. p53 Pulses Diversify Target Gene Expression Dynamics in an mRNA Half-Life-Dependent Manner and Delineate Co-regulated Target Gene Subnetworks. Cell Syst. 2016 Apr 27;2(4):272-82. doi: 10.1016/j.cels.2016.03.006. Epub 2016 Apr 7.
- Poyurovsky MV, Jacq X, Ma C, Karni-Schmidt O, Parker PJ, Chalfie M, Manley JL, Prives C. Nucleotide binding by the Mdm2 RING domain facilitates Arf-independent Mdm2 nucleolar localization. Mol Cell. 2003 Oct;12(4):875-87. doi: 10.1016/s1097-2765(03)00400-3.
- Priest, C., Prives, C., & Poyurovsky, M. V. (2010). Deconstructing nucleotide binding activity of the Mdm2 RING domain. Nucleic Acids Research, 38(21), 7587–7598. https://doi.org/10.1093/nar/gkq669
- Purvis JE, Karhohs KW, Mock C, Batchelor E, Loewer A, Lahav G. p53 dynamics control cell fate. Science. 2012 Jun 15;336(6087):1440-4. doi: 10.1126/science.1218351.
- Richterova, M., R. Stetina, P. Jost, H. Svobodova, V. Rehacek and J. Kassa (2018). "Inter strand crosslinks in DNA induced in vivo by percutaneous application of sulphur mustard to rats and mice." Mutat Res Genet Toxicol Environ Mutagen **832-833**: 35-40.

- Ruff AL, Dillman J 3rd. Sulfur mustard induced cytokine production and cell death: investigating the potential roles of the p38, p53, and NF-kappaB signaling pathways with RNA interference. J Biochem Mol Toxicol. 2010 May-Jun;24(3):155-64. doi: 10.1002/jbt.20321. PMID: 20143454.
- Safarinejad, M. R., S. A. Moosavi and B. Montazeri (2001). "Ocular injuries caused by mustard gas: diagnosis, treatment, and medical defense." Mil Med **166**(1): 67-70.
- Shakarjian, M. P., D. E. Heck, J. P. Gray, P. J. Sinko, M. K. Gordon, R. P. Casillas, N. D. Heindel, D. R. Gerecke, D. L. Laskin and J. D. Laskin (2010). "Mechanisms mediating the vesicant actions of sulfur mustard after cutaneous exposure." <u>Toxicol Sci</u> **114**(1): 5-19.
- Sidell, F. R., E. T. Takafuji and D. R. Franz (1997). <u>Medical aspects of chemical and biological</u> warfare. Washington, D.C., Office of the Surgeon General.
- Solberg, Y., M. Alcalay and M. Belkin (1997). "Ocular injury by mustard gas." <u>Surv Ophthalmol</u> **41**(6): 461-466.
- Song, E. K., Rah, S. Y., Lee, Y. R., Yoo, C. H., Kim, Y. R., Yeom, J. H., Park, K. H., Kim, J. S., Kim, U. H., & Han, M. K. (2011). Connexin-43 hemichannels mediate cyclic ADP-ribose generation and its Ca2+-mobilizing activity by NAD+/cyclic ADP-ribose transport.

  Journal of Biological Chemistry, 286(52), 44480–44490.

  <a href="https://doi.org/10.1074/jbc.M111.307645">https://doi.org/10.1074/jbc.M111.307645</a>
- Speidel D. The role of DNA damage responses in p53 biology. Arch Toxicol. 2015 Apr;89(4):501-17. doi: 10.1007/s00204-015-1459-z. Epub 2015 Jan 25. PMID: 25618545.

- Tarsounas, M., & Sung, P. (2020). The antitumorigenic roles of BRCA1-BARD1 in DNA repair and replication. Nature Reviews. Molecular Cell Biology, 21(5), 284–29 doi.org/10.1038/s41580-020-0218-z
- Tendler, Y., & Panshin, A. (2020). Features of p53 protein distribution in the corneal epithelium and corneal tear film. Scientific Reports, 10(1). https://doi.org/10.1038/s41598-020-67206-z
- Tilley, R. (1993). "The Hydrolysis of Bis(2-chloroethyl) Sulfide (Sulfur Mustard) in Aqueous Mixtures of Ethanol, Acetone, and Dimethyl Sulfoxide." <u>Australian Journal of Chemistry</u> **46**: 293-300.
- Yang, Z., Hanson, R. L., & Batchelor, E. (2021). Progress and challenges in understanding the regulation and function of p53 dynamics. Biochemical Society Transactions, 49(5), 2123–2131. https://doi.org/10.1042/BST20210148
- Yeh, C. D., Richardson, C. D., & Corn, J. E. (2019). Advances in genome editing through control of DNA repair pathways. Nature Cell Biology, 21(12), 1468–1478. https://doi.org/10.1038/s41556-019-0425-z
- Yue, L., Y. Zhang, J. Chen, Z. Zhao, Q. Liu, R. Wu, L. Guo, J. He, J. Zhao, J. Xie and S. Peng (2015). "Distribution of DNA adducts and corresponding tissue damage of Sprague-Dawley rats with percutaneous exposure to sulfur mustard." <a href="#">Chem Res Toxicol</a> 28(3): 532-540.

Footnotes

Affiliations:

1 – Invirsa, Inc., Columbus, OH

2 – Northeastern University, Boston, MA

3 – University of Minnesota, Minneapolis, MN

4 – United States Army Medical Research Institute for Chemical Defense, Baltimore, MD

5 – Wake Forest Institute for Regenerative Medicine, Wake Forest University Health Sciences,

Winston-Salem, NC

Conflicts of Interest

The following authors are affiliated with Invirsa: Robert Shalwitz, Anna Ruehlmann, Alexandrea

Miller and Isaiah Shalwitz

**Financial Support** 

This work was supported by National Institute on Aging of the National Institutes of

Health under award number [Grant K01AG056554] (to TAD); National Institute of

General Medical sciences of the National Institutes of Health under award number [Grant

1R01GM149666] (to EB); funding from the University of Minnesota (to EB); National

Institutes of Health - National Eye Institute [Grant R01EY034139]

Reprint Requests to:

Robert Shalwitz

1275 Kinnear Rd

Columbus OH, 43212

rshalwitz@invirsa.com

Figure Captions:

**Figure 1:** Effects of INV-102 on levels of key regulators of DNA damage response pathways and corneal epithelial cell differentiation. HCEC were treated with INV-102 at 60 μM for 15, 30, 60, or 120 minutes and levels of p53 (A), Sirt6 (B), and Pax6 and cytokeratin-12 (C) were compared to untreated controls via immunoblot. Percent increase is expressed relative to the no treatment band. Each lane was loaded with equal amounts of total protein.

**Figure 2:** Mean + Standard error expression profile of p53-Venus expression (MSE) in hTERT-RPE-1 cells (n=50) in response to INV-102 (Red) compared to levels in untreated hTERT-RPE-1 cells (n=11) (Blue). Measurements were first taken 20 minutes after the addition of INV-102 which may account for the difference in initial values.

Figure 3: qPCR results following treatment with INV-102 of mean gene expression ± standard error for multiple proteins involved in DNA repair. \* p < 0.05, \*\* p < 0.01, \*\*\* is p < 0.001. A) qPCR for proteins known to be modulated by p53. B) qPCR for proteins known to be important for homologous recombination. qPCR levels were collected over at 0, 4, 8, and 24 hours following INV-102 treatment. Results were measured from start of treatment with INV-102. The treatment was removed at the 4-hour timepoint. Data is presented as mean log 2-fold change ±SEM.

**Figure 4:** Use of reporters to show the recruitment of BRCA following DSB **A)** Measurement of BRCA recruitment following DSB by Attune NxT flow cytometer. The distance of BRCA1 from the DSB site was measured in bp and shown to be significantly increased by INV-102 compared to vehicle at 100 μM. **B)** DR-GFP reporter pathway. **C)** The frequency of the DR-GFP reporter was measured at 50 and 100 μM of INV-102 as well as control. INV-102 treated cells show a

significant increase in frequency of GFP positive cells following Iscel treatment compared to vehicle. **D)** Measurement of Cleavage levels by I-Scel indicating INV-102 shows no alteration of cleavage levels by Iscel.

**Figure 5: A)** Kinetics of  $\gamma$ H2AX focus formation following bleomycin examined by immunofluorescence. At 2 hours, INV-102 cells had significantly increased  $\gamma$ H2AX foci, but by 4 hours they were significantly decreased. This indicates that INV-102 shortens the entire time course of  $\gamma$ H2AX focus recruitment and resolution. **B)** Cell cycle distribution profiles of vehicle and INV-102 treated cells. The cell cycle distribution profiles of vehicle-treated and INV-102-treated cells were nearly identical.

**Figure 6:** Clinical observations of vehicle-treated (n=15) and INV-102-treated (n=15) rabbit eyes from 0-70 d post-exposure. **A)** Bright field images (top) and fluorescein uptake (bottom, a measure of epithelial integrity) for representative vehicle-treated and INV-102-treated eyes from 0-70 d post-exposure. **B)** Mean corneal thickness as measured by ocular coherence tomography (OCT). **C)** Clinical severity scores. **D)** Opacity scores. **E)** Fluorescein uptake scores. For B-E, the short bar from 1-14 d represents treatment with INV-102 or vehicle. Time points at which significant differences exist between the two treatment conditions are annotated with a line and the corresponding maximum p-value.

Figure 7: Effects of treatment on corneal morphology. (A) Longitudinal changes in representative corneas imaged by optical coherence tomography (OCT). Note the emergence of edematous voids during the recurrent edematous lesion in vehicle treated eyes. (B) Vehicle-treated and INV-102-treated corneas were enucleated at 10 wk after SM exposure and corneal morphology was visualized with hematoxylin and eosin. A naïve cornea is shown for

comparison. Note areas of fibrosis (f) in vehicle-treated cornea, indicated by increased eosin intensity and matrix disorganization. (C) A higher magnification view of the regions annotated by boxes in panel B. v = blood vessel; d = disorganized tissue structure in stroma or epithelium; c = inflammatory cell infiltrates.

Table 1: Primers used for rt-PCR

| Gene    | Forward Primer           | Reverse Primer           |
|---------|--------------------------|--------------------------|
| RAD51   | CGAGCGTTCAACACAGACCA     | GTGGCACTGTCTACAATAAGCA   |
| BRCA1   | GGCTATCCTCTCAGAGTGACATTT | GCTTTATCAGGTTATGTTGCATGG |
| BRCA2   | GAAAATCAAGAAAAATCCTTAAA  | GTAATCGGCTCTAAAGAAACATG  |
|         | GGCT                     | ATG                      |
| CDKN1A  | TACCCTTGTGCCTCGCTCAG     | ATCAGCCGGCGTTTGGAGTG     |
| MDM2    | TAGGAGATTTGTTTGGCGTGC    | CTGAGTCCGATGATTCCTGCT    |
| GADD45A | TGCTGGTGACGAATCCACATT    | TGATCCATGTAGCGACTTTCCC   |
| MSH2    | GTCACAGCACTCACCACTGA     | AGCTCTGCAACATGAATCCCA    |
| MLH1    | GAGCAGGGACATGAGGTTCT     | ACTTGGTTTGATGCTGTGCC     |
| BAX     | CTGACGGCAACTTCAACTGG     | GATCAGTTCCGGCACCTTGG     |
| FANCC   | AAGGTCTTGGGTATGCACCT     | GGAGCCATTCGCCTTTGAGT     |
| XPC     | TCTTCGGAGGGCGATGAAAC     | TCTTCGGAGGGCGATGAAAC     |
| RRM2B   | TTGGGCCTTGCGATGGATAG     | GTGAGTCCTGGCATAAGACCT    |
| DDB2    | TCATTGTTGTGGGCCGATAC     | TGGCTCCAGATGAGAATGTG     |
| PCNA    | TGAAGCACCAAACCAGGAGA     | GTGCAAATTCACCAGAAGGCA    |

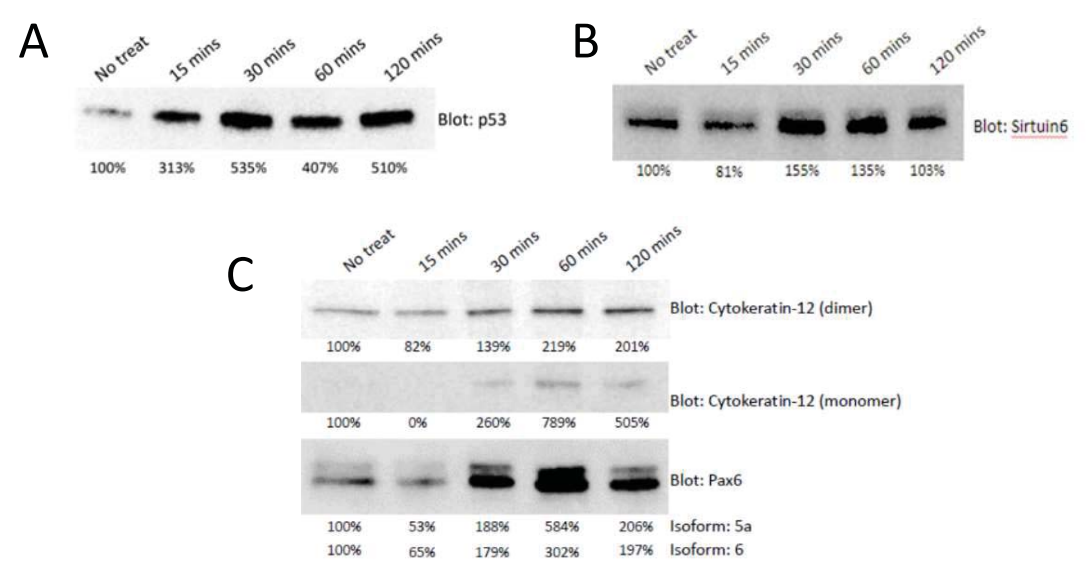


Fig. 1

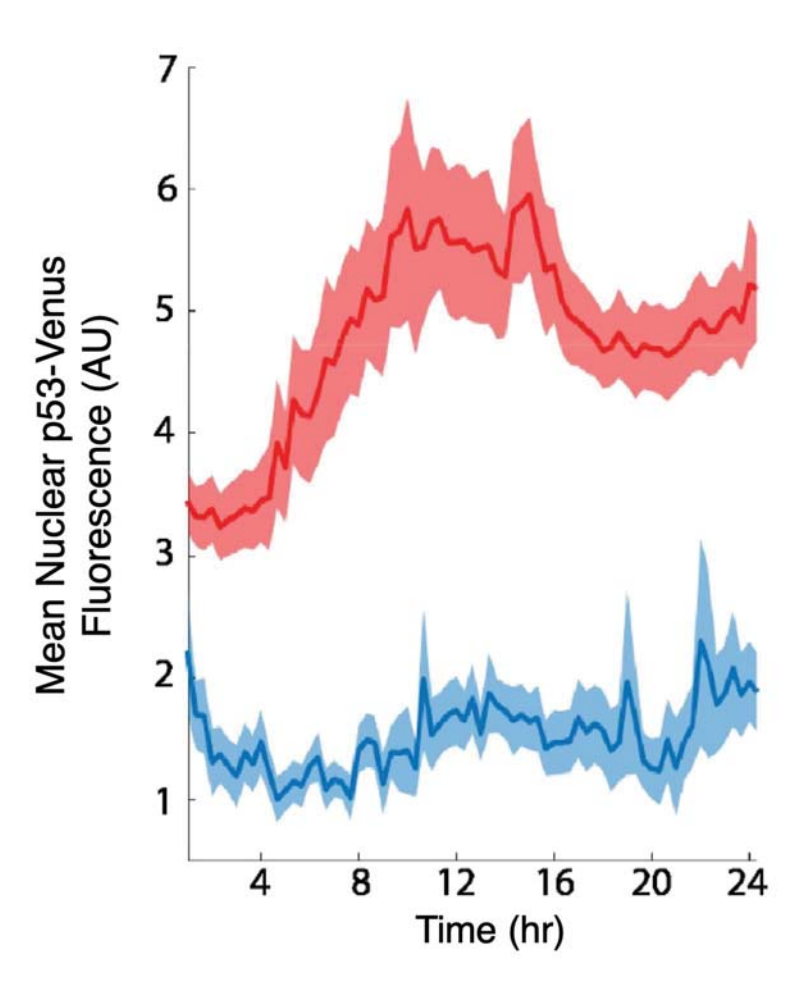


Fig. 2

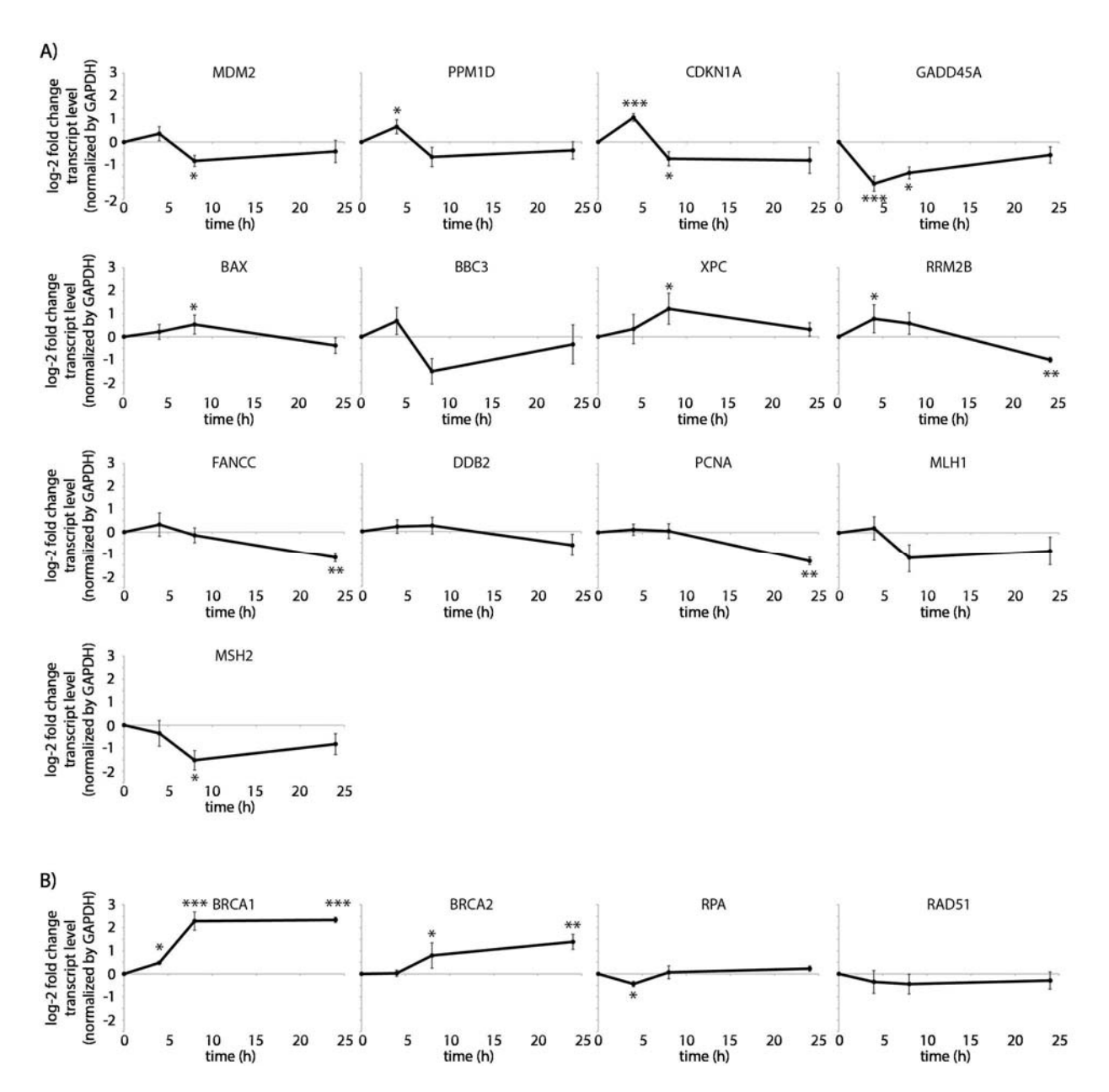


Fig. 3

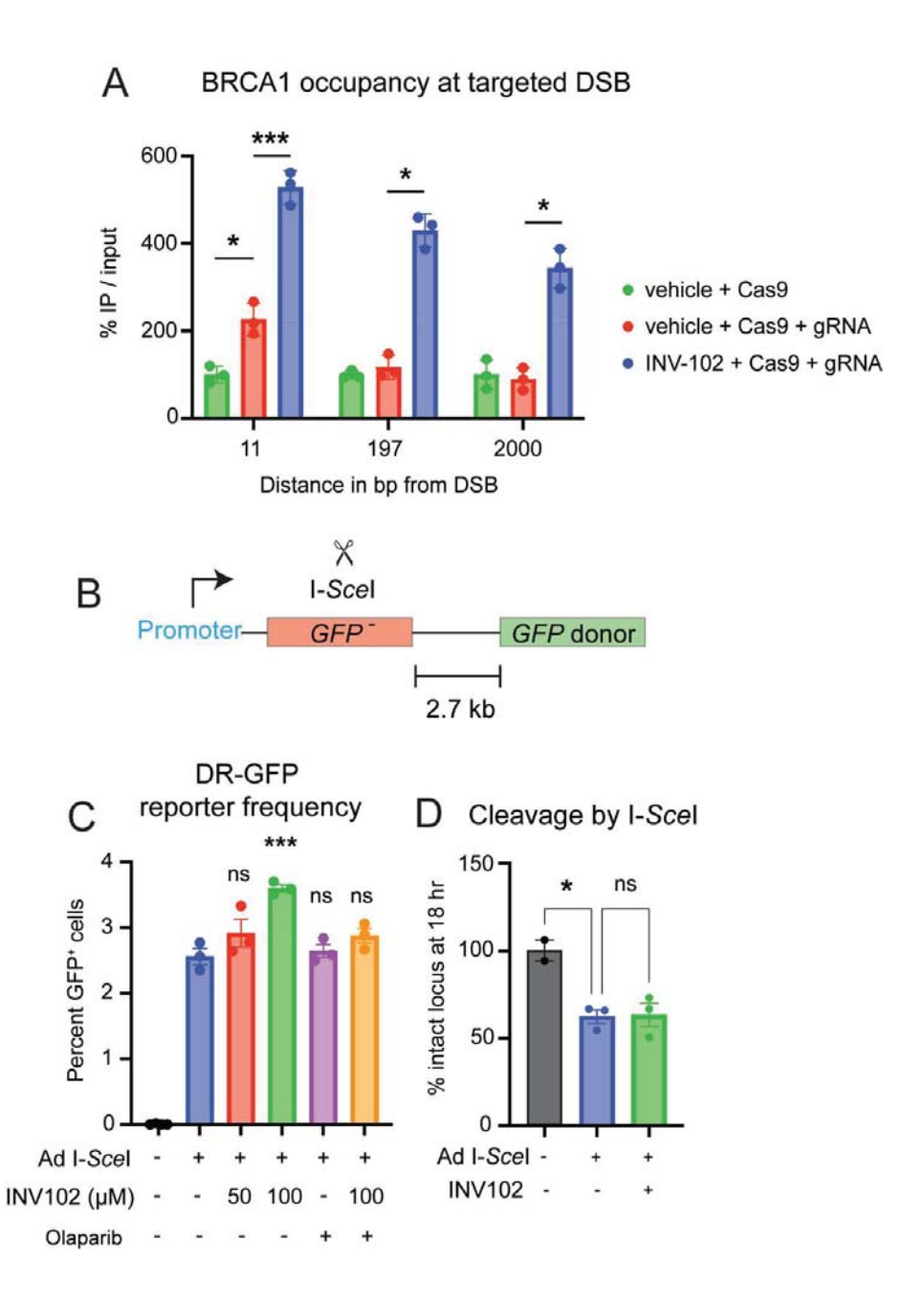


Fig. 4

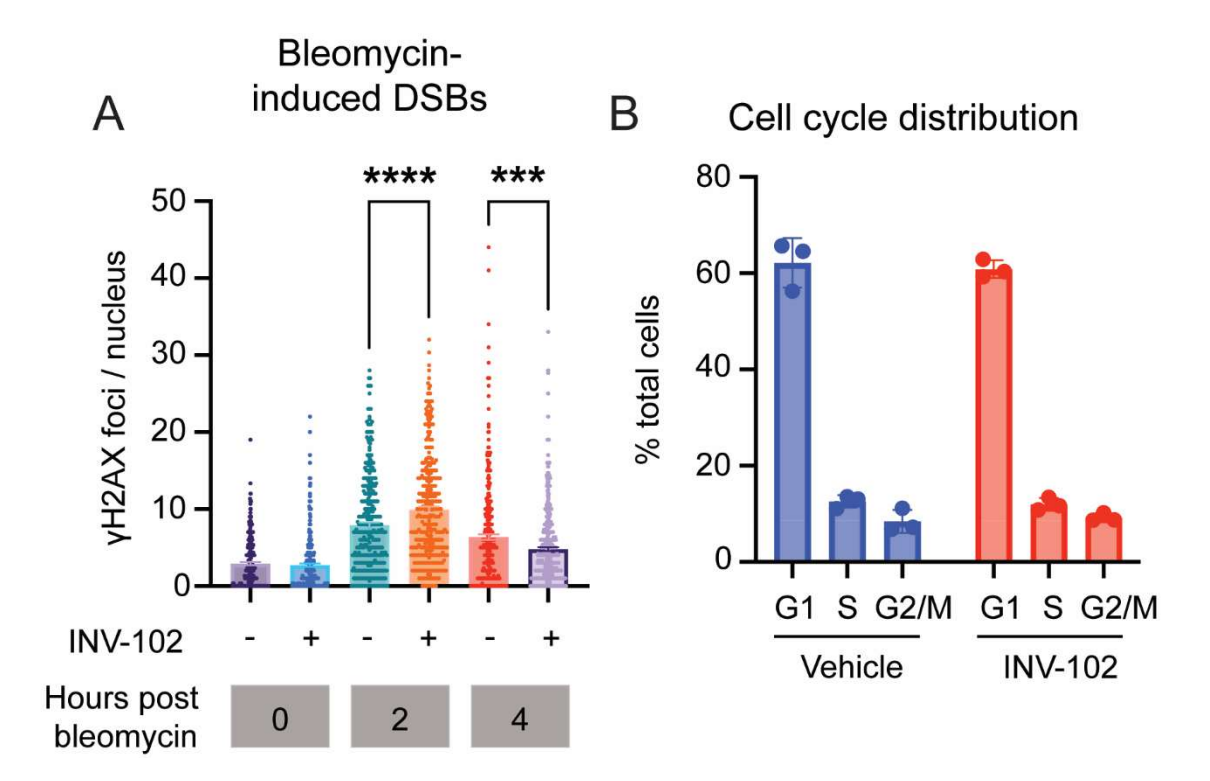


Fig. 5

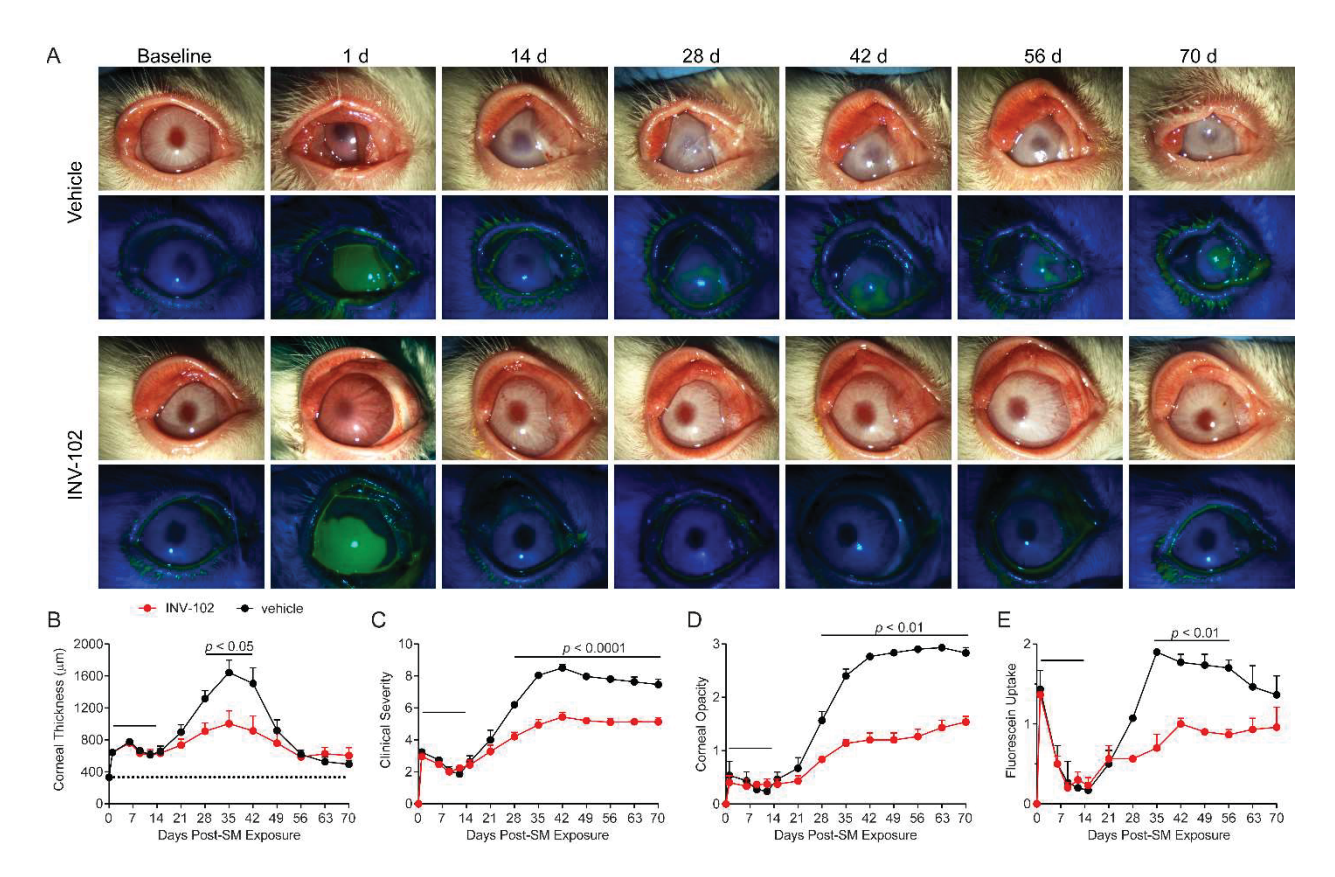
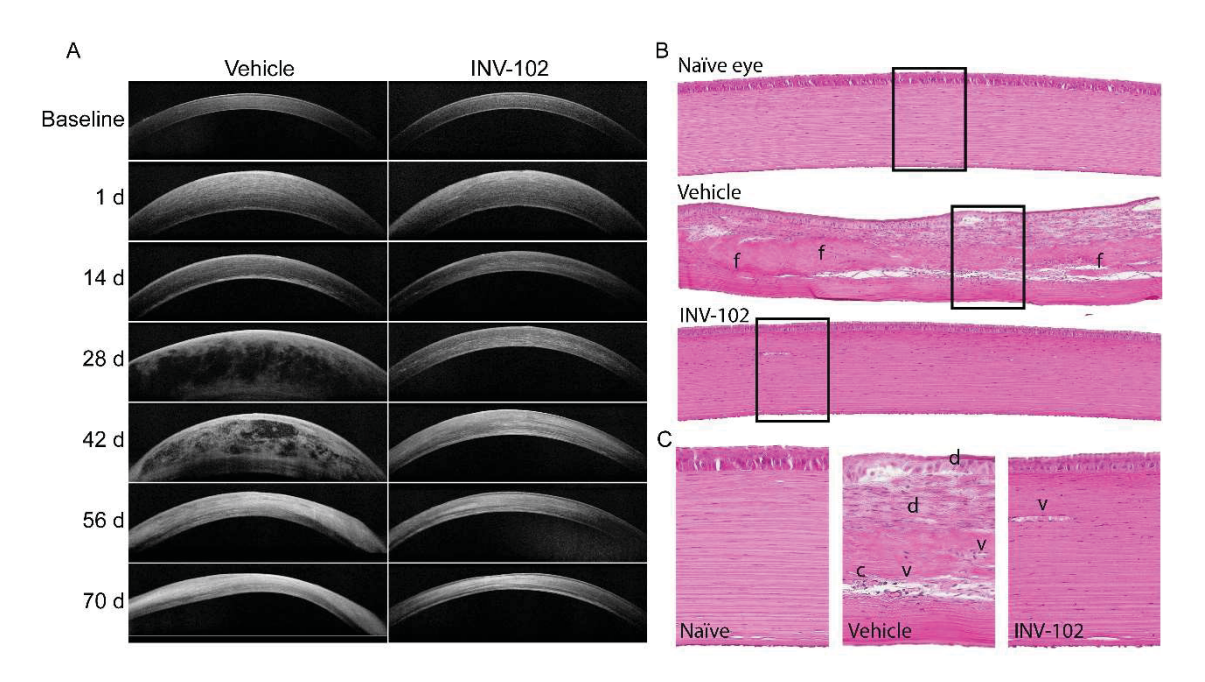


Fig. 6



**Fig.** 7